International Journal of Minerals, Metallurgy and Materials
Volume 22, Number 11, November 2015, Page 1149
DOI: 10.1007/s12613-015-1179-7

Effect of electroslag remelting on carbides in 8Cr13MoV martensitic stainless steel

Qin-tian Zhu, Jing Li, Cheng-bin Shi, and Wen-tao Yu

State Key Laboratory of Advanced Metallurgy, University of Science and Technology Beijing, Beijing 100083, China
(Received: 4 August 2014; revised: 30 December 2014; accepted: 5 January 2015)

Abstract: The effect of electroslag remelting (ESR) on carbides in 8Cr13MoV martensitic stainless steel was experimentally studied. Phases precipitated from liquid steel during solidification were calculated using the Thermo-Calc software. The carbon segregation was analyzed by original position analysis (OPA), and the carbides were analyzed by optical microscopy (OM), scanning electron microscopy (SEM), energy-dispersive X-ray spectroscopy (EDS) and X-ray diffraction (XRD). The results indicated that more uniform carbon distribution and less segregation were obtained in the case of samples subjected to the ESR process. After ESR, the amount of netty carbides decreased significantly, and the chromium and vanadium contents in the grain-boundary carbides was reduced. The total area and average size of carbides were obviously smaller after the ESR process. In the sample subjected to ESR, the morphology of carbides changed from lamellar and angular to globular or lump, whereas the types of carbides did not change; both $M_{23}C_6$ and M_7C_3 were present before and after the ESR process.

Keywords: martensitic stainless steel; electroslag remelting; carbides

1. Introduction

8Cr13MoV is a martensitic stainless steel with high hardness and wear resistance; it can be used as a senior material for razor blades. Electroslag remelting (ESR) is a special smelting method with dual functions of solidification and refining [1]. It can alleviate segregation and result in a uniform structure [2−6].

Carbon is used as an alloying element in stainless steel; it serves an important function of strengthening the performance of steel and stabilizing austenite [7−8]. With increasing carbon content, both the hardness and the wear resistance of steel improve consistently. However, increased carbon content can cause an increase in the concentration of carbides, which reduces the corrosion resistance of steel [9]. In the case of high-alloy steels, segregation of the alloying elements easily occurs during the solidification of liquid steel. As a result, numerous primary carbides precipitate in the steel, including some netty carbides distributed along the grain boundaries. Research has shown that an increase in the content of alloying elements will induce the aggregation and growth of carbides [10]. These carbides are not easy to diminish, and they will adversely affect the durability and fatigue resistance of steel.

The ESR process has been widely used in the production of high-carbon materials used for knives or scissors. Dorschu advocated smelting of M2 high-speed steel using ESR. His research indicated that the ESR process can reduce the size of carbides, and Kirk hypothesized that ESR could alleviate the segregation of carbides in M2 high-speed steel [11]. However, the effect of ESR on carbides in martensitic stainless steel with a high carbon content has not been reported. In this paper, carbides in 8Cr13MoV steel were studied by experiments and by thermodynamic calculations.

2. Experimental

The ordinary as-cast steel used in this paper was 8Cr13MoV with the composition shown in Table 1. The

Corresponding author: Jing Li E-mail: lijing@ustb.edu.cn

as-cast steel was forged into electrode bars 800 mm in length and 25 mm in diameter. A 10-kg-scale ESR furnace was used to remelt the electrode bars. The alternating current intensity was 750 A, and the slag included 60wt% CaF_2, 20wt% CaO, and 20wt% Al_2O_3. Several specimens with dimensions of 12 mm × 12 mm × 12 mm were cut from the original cast ingot and from the ESR ingot. Both kinds of specimens were taken from the half-radius of the ingots. Carbon segregation in the transverse section of both ingots was analyzed using an original position analyzer. Optical microscopy (OM) and scanning electron microscopy (SEM) were used to observe the microstructures of samples after the samples were ground, polished, and eroded. Several round rods 80 mm in length and 15 mm in diameter were cut from steel samples before and after the samples were subjected to ESR. Electrolysis was conducted to extract carbides from the steel. In the electrolytic experiments, round samples were used as the anode and a copper sheet was used as the cathode. The electrolyte was an organic solution. The current density was maintained at less than 100 mA/cm^3. After the completion of the electrolytic experiments, each of which lasted for 6 h, the carbide powder was vibrated loose from the round rods using an ultrasonic cleaning machine. The carbide powder was then elutriated with deionized water. X-ray diffraction (XRD) and SEM were used to analyze the composition and morphology of the carbides. The content of alloying elements in the carbides was analyzed by energy-dispersive X-ray spectroscopy (EDS). Tensile tests were performed using a universal material testing machine.

Table 1. Chemical composition of 8Cr13MoV martensitic stainless steel investigated in this study wt%

C	Si	Mn	P	S	Cr	Ni	Mo	V	Fe
0.775	0.333	0.458	0.031	0.004	14.18	0.157	0.213	0.182	Bal.

3. Results and discussion

3.1. Effect of ESR on carbon segregation

The content of each element at any position and its distribution in the transverse section of the ingots was obtained directly and with high accuracy by original position analysis (OPA) [12]. OPA is a method based on continuous excitation spark spectroscopy with two-dimensional scanning of specimens, high-speed signal acquisition of single spark discharge, and data analysis [13]. The OPA instrument can scan large-sized specimens and generate signals reflecting both the concentrations and locations of the elements in the scanned areas.

In this study, an OPA-200 instrument was used to analyze the carbon segregation in 8Cr13MoV martensitic stainless steel. The scanning method was linear scanning at a speed of 1 mm/s. Samples with a transverse section size of 30 mm × 30 mm were taken from the half-radius of a traditional ingot and an ESR ingot. The results are shown in Fig. 1.

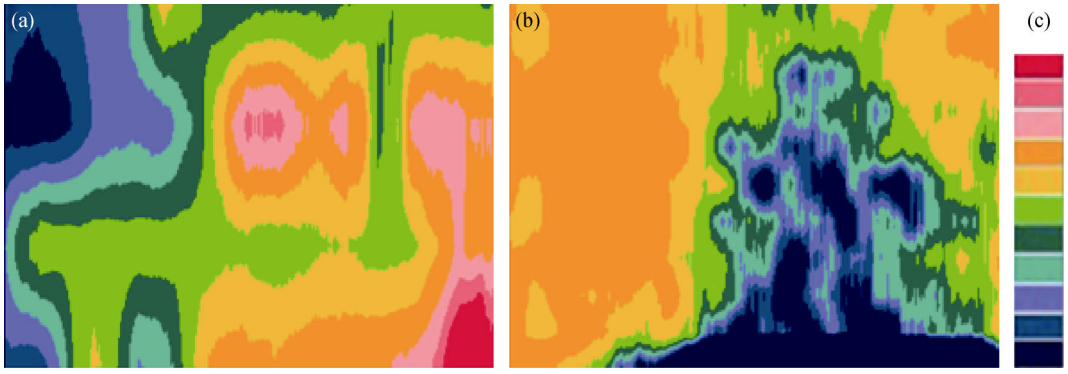

Fig. 1. Carbon distribution maps in the transverse section of different ingots: (a) traditional ingot; (b) ESR ingot; (c) a color bar indicating that the carbon concentration decreases as the color changes from red to blue.

The red and pink regions in Fig. 1 indicate the areas of serious carbon segregation, whereas the yellow and earthy-yellow parts indicate the areas of uniform carbon distribution. The results indicate that more uniform carbon distribution and less segregation were obtained in the case of the ingot subjected to the ESR process. The carbon segregation area can provide conditions that favor the formation of carbides. Less carbide segregation should occur in the ESR ingot; this prediction was verified in the subsequent study presented in this paper.

3.2. Effect of ESR on the number and morphology of carbides

Fig. 2 shows the specimens eroded by alkaline supersaturated potassium permanganate. The major function of potassium permanganate is to erode carbides. As shown in

Fig. 2, most carbides in the traditional ingot precipitated continuously and with an angular morphology along grain boundaries. In contrast, the morphology of carbides in the ESR ingot was globular or lump-like. The grain boundaries were indistinct as a result of the obvious decrease in the amount of carbides precipitated along grain boundaries. Most carbides were discretely distributed in the interior of grains.

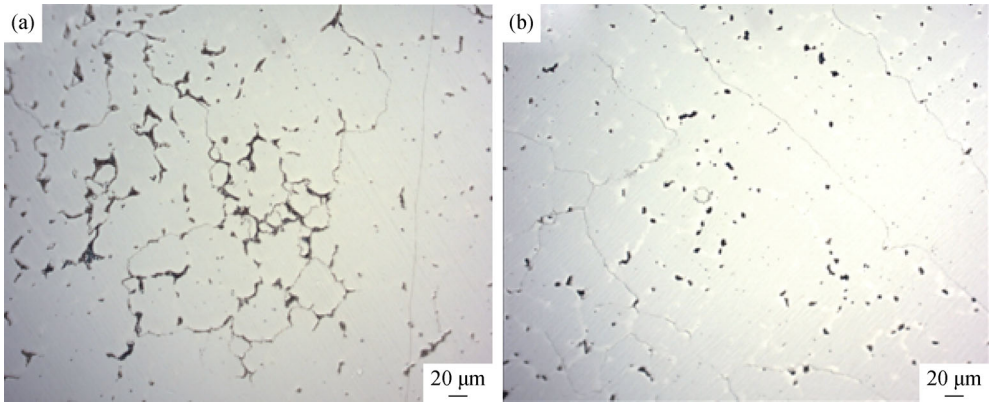

Fig. 2. Carbides in the traditional ingot (a) and ESR ingot (b).

Five different fields of view were selected randomly; the area of each field was 0.2 mm^2. The total area, average diameter, and roundness of the carbides were then measured using the Image-ProPlus software. The results, which are shown in Table 2, indicate that the total area and average diameter of the carbides in the ESR ingot decreased significantly and that their roundness improved.

Table 2. Number and shape parameters of carbides

Measurement items	Number	Total area / μm^2	Diameter / μm	Roundness
Before ESR	298	4225.36	4.25	3.02
After ESR	190	2059.12	3.32	2.12

At present, the ESR process is not used in the manufacture of low-carbon martensitic stainless steels. However, ESR is necessary when the carbon content exceeds 0.6wt%. As evident in Fig. 2, the amount of carbides precipitated from the matrix was reduced significantly in the ingot subjected to ESR. In addition, as shown in Table 2, the ESR process reduced the average diameter of carbides from 4.25 μm to 3.32 μm. If the average diameter is used to express the size of carbides, then the size of the carbides was decreased by 22%.

Under the experimental conditions, the process used to cool the traditional ingot was air cooling, whereas the ESR ingot was cooled in a water-refrigerated copper crystallizer. Hence given that the samples were collected from the same position, the cooling intensity of ESR was greater than that of the traditional process. This result indicates that the ESR process improved the cooling rate and alleviated carbon segregation, which, as verified by the OPA results in Fig. 1, consequently reduced the precipitation of proeutectoid cementites at the grain boundaries before the generation of pearlite. As a consequence, carbon atoms could dissolve in the matrix more uniformly. Fine dispersed carbides are more easily created during the process of hot rolling and spheroidizing annealing, and the presence of these carbides facilitates the re-dissolution of carbides during the austenitization stage of quenching. Thus, an opportunity exists to avoid the problems associated with coarse grains caused by high quenching temperatures or long holding time [14]. In conclusion, ESR provides better heat-treatment conditions, which leads to grain refinement.

In addition, as shown in Fig. 2, some primary carbides were observed in the ingot solidified using the traditional process. These primary carbides exhibit large sizes and irregular shapes and are difficult to remove during a heat treatment [15]. In addition, the presence of large carbides is likely to cause stress concentration, thereby degrading the performance of the steel. After ESR, the amount of primary carbides was obviously reduced. Therefore, in the case of high-carbon martensitic stainless steels, the use of ESR is necessary to reduce the precipitation of primary carbides.

Fig. 3 shows the carbides extracted from steel by electrolytic extraction. As evident in Fig. 3, the morphology of carbides in the sample not subjected to ESR was either lamellar or angular and their appearance was relatively sharp. However, carbide particles in the sample subjected to ESR became smaller and exhibited a globular or lump-like morphology and a relatively smooth appearance.

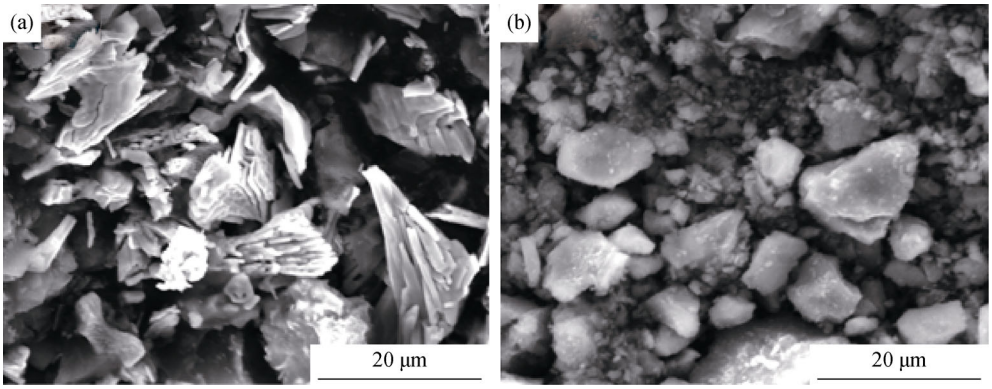

Fig. 3. Morphologies of carbides extracted from the traditional ingot (a) and ESR ingot (b).

In the case of hyper-eutectoid steels such as 8Cr13MoV, a low cooling rate results in the precipitation of proeutectoid cementites along the grain boundaries. The carbides can grow in a certain direction because of stress at the grain boundaries, and they have sufficient time to grow. Therefore, as observed in the experiments, these carbides are large and exhibit a lamellar and angular morphology. In contrast, the cooling intensity of ESR is very strong, which inhibits the diffusion of alloy elements during solidification. Only a few precipitated proeutectoid cementites were observed along the grain boundaries. Austenite with a hypereutectoid composition transforms to pearlite directly. These carbides in pearlite have little time to grow. In addition, they form in the interior of the grains, and therefore no stress is introduced by grain boundaries. Consequently, these carbides are small and exhibit a globular or lump morphology. Lamellar carbides cannot be easily broken during the rolling process, and angular carbides are likely to cause stress concentration, which reduces the toughness and strength of steel. Therefore, ESR improves the morphology of carbides, which thereby makes the thermal processing and heat treatment of the steel more convenient.

3.3. Effect of ESR on grain-boundary carbides

Fig. 4 shows the microstructures of steel samples before and after the ESR process. Before ESR, the microstructure includes pearlite and netty carbides precipitated along the grain boundaries. However, after ESR, the microstructure consists of pearlite, retained austenite, and some tufted carbides, whereas the quantity of netty carbides decreases dramatically. The reason for these differences in microstructure is that ESR inhibits the precipitation of proeutectoid cementites, which results in the austenite with a hypereutectoid composition transforming to pearlite directly. This kind of pearlite is called pseudopearlite. Because of its high carbon content, this austenite with a hypereutectoid composition is highly stable [16–17]. As a result, some austenite is retained after the phase transition.

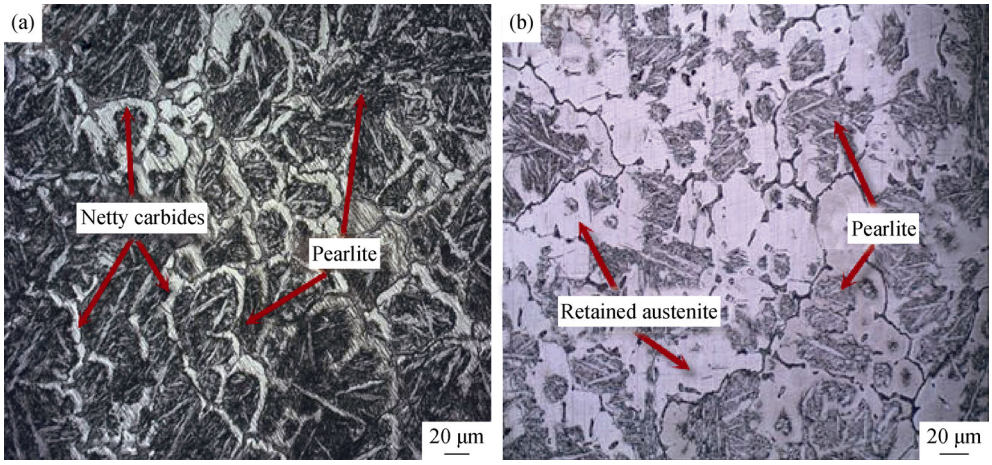

Fig. 4. Microstructures of the traditional ingot (a) and ESR ingot (b).

Fig. 5 shows the effect of ESR on the carbides at grain boundaries. As shown in Fig. 5, before ESR, carbides at the grain boundary are thick and large. After ESR, the carbides distribute in the grain boundary discontinuously and some tufted chromium carbides are observed in the matrix. The amounts of chromium and vanadium in grain-boundary car-

bides were measured. Six points on the components in the grain-boundary carbides of the traditional ingot and the ESR ingot were randomly selected. The average contents are shown in Table 3, which reveals less segregation of alloying elements at the grain boundaries after ESR.

3.4. Effect of ESR on the properties of steel

As previously noted, the effect of ESR on the quantity, size, and morphology of carbides is obvious. Given that the microstructure of steels governs the steels' properties, two groups of tensile experiments based on GB/T 228.1—2010 were performed. In each group of experiments, measurements of three tensile samples 70 mm in length and 6 mm in diameter were performed, and the average tensile strength was calculated. The results show that the tensile strengths of the traditional sample and the ESR sample were 792 MPa and 1161 MPa, respectively. The improvement of tensile strength was immense.

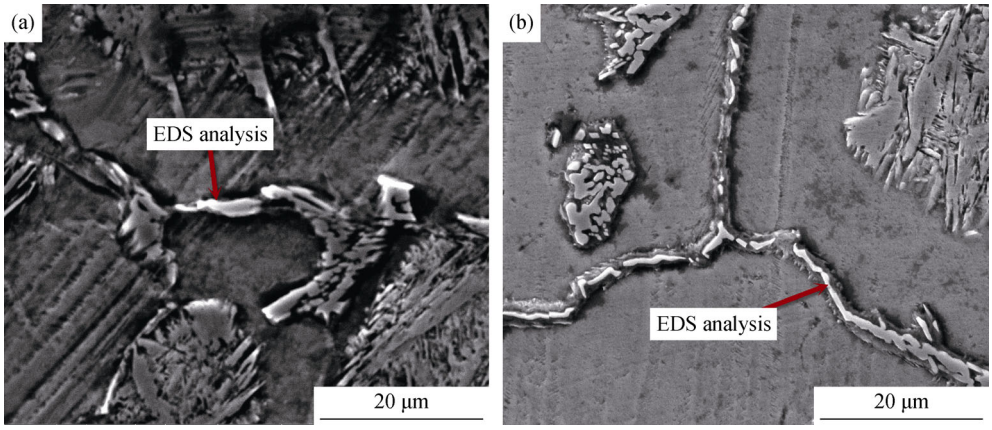

Fig. 5. SEM images of boundary carbides: (a) traditional ingot; (b) ESR ingot.

Table 3. EDS analysis results for boundary carbides wt%

Elements	Fe	Cr	C	V
Before ESR	49.25	42.71	7.12	0.95
After ESR	54.01	37.86	7.68	0.45

As is well known, carbon is a very important element for improving the strength of steel. According to Table 2, the quantity of carbides decreased by 51% after ESR. Therefore, more carbon dissolved in the matrix of the steel, which resulted in solution strengthening. In addition, as shown in Fig. 6, the fracture surfaces of the samples before ESR contained more large carbides, which could easily lead to stress concentration and material cracking. More important, as shown in Fig. 4, the netty carbides precipitated at the grain boundaries in traditional steel severely deteriorated the steel's tensile strength, which could easily lead to intergranular fracture. On the basis of these points, the tensile strength of steels subjected to ESR should be greatly improved.

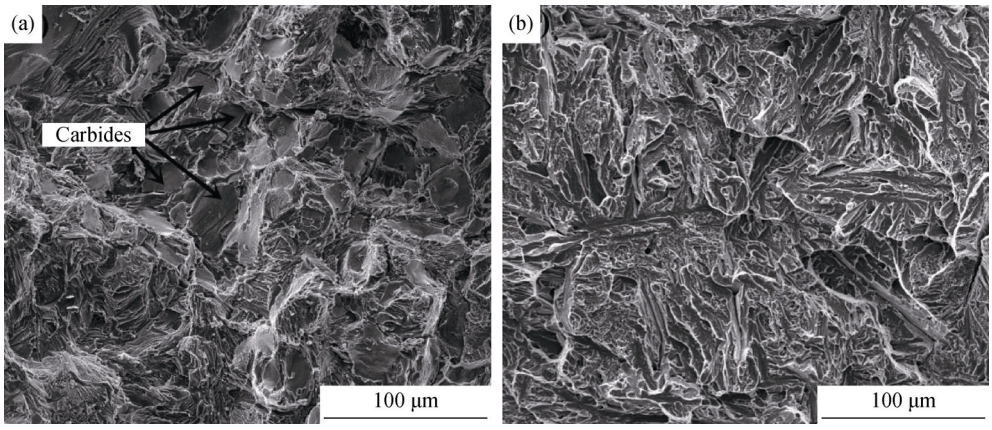

Fig. 6. Fracture surfaces of the traditional ingot (a) and ESR ingot (b).

3.5. Effect of ESR on the types of carbides

In this study, the Thermo-Calc program was used to calculate the phase equilibrium and transitions during the solidification of liquid steel. Thermo-Calc is a useful tool in iron and steel research; it can be used to perform various

thermodynamic calculations of, for example, the equilibrium phase composition of steels, the effects of alloying, and the forming law of precipitated phases. According to the composition of the steel used in our experiments, the precipitated phases and the transitions between phases were calculated for the temperature interval of 400 to 1600°C on the basis of the TCFE5 database in Thermo-Calc. The results are presented in Fig. 7. As shown in Fig. 7, the liquidus temperature of this stainless steel is 1430°C. The peritectic reaction, δ-ferrite + L → γ-Fe, occurs at 1415°C. When the temperature reaches 1400°C, the peritectic reaction ends and the liquid steel begins to transform into austenite. At 1320°C, the liquid steel is solidified completely as a single austenite phase. M_7C_3 (M represents metal elements) carbides begin to precipitate from austenite at 1240°C. The number of M_7C_3 precipitates reaches a maximum at 920°C, and M_7C_3 simultaneously begins to transform into $M_{23}C_6$; this transition is complete at 760°C. Also, the austenite starts to transform into α-ferrite when the temperature reaches 810°C. Finally, the microstructure transforms into α-ferrite and $M_{23}C_6$.

Fig. 8 shows the curves for the mass fraction of each element as a function of temperature. The existing intervals for $M_{23}C_6$ and M_7C_3 are 0–920°C and 760–1240°C, respectively. As evident in Fig. 8, the content of Fe in $M_{23}C_6$ decreases during the temperature interval where M_7C_3 changes to $M_{23}C_6$ with decreasing temperature. After this transition, the rate of decrease accelerates. As the temperature decreases from 920 to 760°C, the chromium content continues to increase; the rate of increase of chromium content then accelerates as the temperature is decreased further. In the case of M_7C_3, as the temperature decreases, the Fe content decreases and the Cr content increases. The carbon content in M_7C_3 and $M_{23}C_6$ does not change throughout the solidification process.

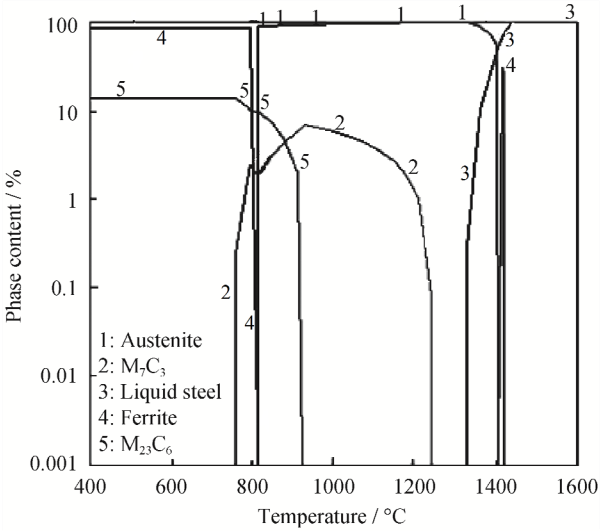

Fig. 7. Precipitated phases and transitions between phases in the temperature range from 400 to 1600°C.

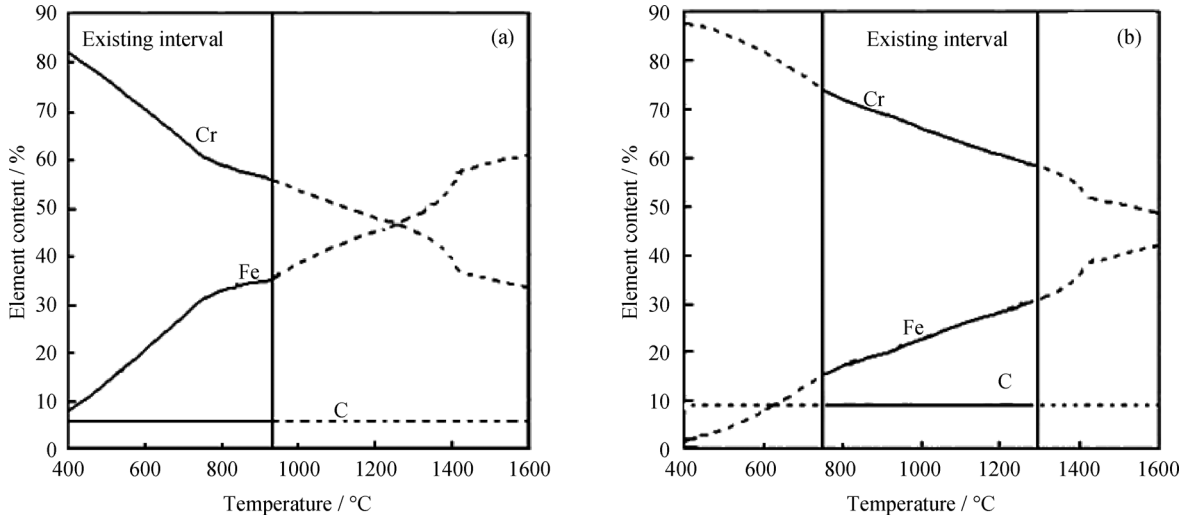

Fig. 8. Content of each element in two types of carbides with decreasing temperature: (a) $M_{23}C_6$ and (b) M_7C_3.

As also evident in Fig. 8, with decreasing temperature, chromium atoms tend to spread to carbides and replace Fe atoms spontaneously. This process might inevitably lead to a decrease in the chromium content in the steel matrix, thereby reducing the corrosion resistance of the material. As previously mentioned, ESR provides greater cooling intensity relative to the ordinary solidification process in these experiments. Hence, the diffusion of alloy elements is suppressed during the solidification of liquid steel. We conclude that the ESR process can reduce the content of chromium in carbides. In actual production, the current intensity can be suitably reduced to control a shallow metal pool and shorten the local

solidification time, thereby improving the cooling intensity indirectly and reducing the segregation of alloying elements.

XRD was used to analyze the extracted carbides. As is shown in Fig. 9, the types of carbides present were $M_{23}C_6$ and M_7C_3 before and after ESR. The ESR process did not change the type of carbides. According to thermodynamic calculations, M_7C_3 carbides precipitate first at 1240°C. With decreasing temperature, M_7C_3 will convert into $M_{23}C_6$ at 920°C and this transition will be complete at 760°C; finally, only $M_{23}C_6$ will exist. However, the experimental results show that both carbides were present in the ingots before and after ESR.

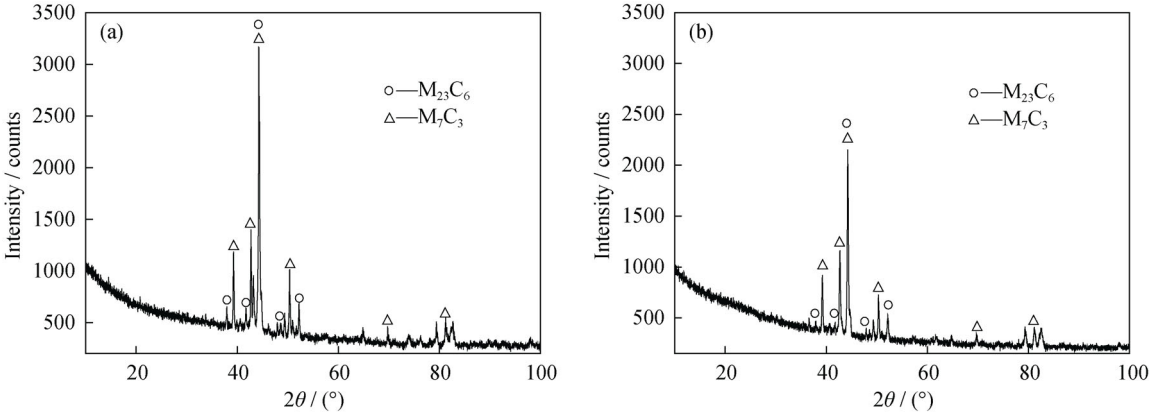

Fig. 9. XRD analysis of carbides extracted from the traditional ingot (a) and ESR ingot (b).

The discrepancy between Thermo-Calc calculation results and experiment results is explained as follows: The results calculated using Thermo-Calc represent the thermodynamic equilibrium state at each temperature. In the whole calculation, the dynamics condition is ideal and element segregation is not considered. In the experiments, whose results differ from those of Thermo-Calc, we could only observe and analyze final phases under different production processes; nonetheless, the results were closer to the authentic phenomenon. However, experiments cannot reflect the whole process of precipitation and transition of each phase. In this study, the experiments showed that M_7C_3 and $M_{23}C_6$ were both present in the final microstructure, whereas the Thermo-Calc calculation results indicated that only $M_{23}C_6$ should exist. According to the calculations, M_7C_3 will transform into $M_{23}C_6$ as the temperature decreases from 920 to 760°C. As is well known, the transition of carbides results from the diffusion of alloying elements and reorganization of the lattice. Under the conditions of actual solidification, because the complete diffusion of alloying elements cannot be completed, M_7C_3 can only partially transform into $M_{23}C_6$. Hence, $M_{23}C_6$ and M_7C_3 coexist.

4. Conclusions

(1) A microstructure with less segregation and fewer netty carbides can be obtained via the ESR process.

(2) After ESR, the total area and average size of carbides obviously decrease and the chromium and vanadium contents in the grain-boundary carbides are reduced. The morphology of the carbides changes from lamellar and angular to globular or lump.

(3) The types of carbides do not change. Both $M_{23}C_6$ and M_7C_3 exist before and after ESR.

(4) On the basis of Thermo-Calc calculation results, Cr atoms tend to diffuse into carbides and replace Fe atoms spontaneously with decreasing temperature during the process of solidification.

Acknowledgements

This work was financially supported by the National Natural Science Foundation of China (No. 51444004), and China Postdoctoral Science Foundation (No. 2014M560047).

References

[1] M.Q. Chen, B.K. Li, and L. Zhao, The cellular automata model of electroslag remelting ingot structure, *J. Mater. Metall.*, 10(2011), p. 130.

[2] Z.B. Li, *Electroslag Metallurgy Theory and Practice*, Metallurgical Industry Press, Beijing, 2010, p. 66.

[3] Z.F. Ni, Y.S. Sun, F. Xue, J. Zhou, and J. Bai, Evaluation of electroslag remelting in TiC particle reinforced 304 stainless steel, *Mater. Sci. Eng. A*, 528(2011), No. 11, p. 5664.

[4] Q.L. Wu, Y.S. Sun, F. Xue, and J. Zhou, Microstructure, mechanical and wear properties of TiC particulate reinforced 2Cr13 steel by *in situ* reaction and electroslag remelting, *Ironmaking Steelmaking*, 35(2008), No. 5, p. 387.

[5] Y.W. Dong, Z.H. Jiang, and Z.B. Li, Segregation of niobium

during electroslag remelting process, *J. Iron Steel Res. Int*., 16(2009), No. 1, p. 7.

[6] H. Halfa, Characterization of electroslag remelted super hard high speed tool steel containing niobium, *Steel Res. Int*., 84(2013), No. 5, p. 495.

[7] J.Y. Park and Y.S. Park, The effects of heat-treatment parameters on corrosion resistance and phase transformations of 14Cr–3Mo martensitic stainless steel, *Mater. Sci. Eng. A*, 449-451(2007), p. 1131.

[8] J.W. Lee and J.T. Kim, The effect of Co–N addition on mechanical properties, microstructure and erosion of 17Cr steels, *ISIJ Int*., 48(2008), No. 1, p. 114.

[9] A. Bhattacharya and P.M. Singh, Effect of heat treatment on corrosion and stress corrosion cracking of S32205 duplex stainless steel in caustic solution, *Metall. Mater. Trans. A*, 40(2009), No. 6, p. 1388.

[10] K.H. Kim, S.D. Park, and C.M. Bae, New approach to the soaking condition of 100Cr6 high-carbon chromium bearing steel, *Met. Mater. Int*., 20(2014), No. 2, p. 207.

[11] J.M. Xiao, *Metallography Issue of Stainless Steel*, Metallurgical Industry Press, Beijing, 2006, p. 41.

[12] H.J. Wu, N. Wei, Y.P. Bao, G.X. Wang, C.P. Xiao, and J.J. Liu, Effect of M-EMS on the solidification structure of a steel billet, *Int. J. Miner. Metall. Mater.*, 18(2011), No. 2, p. 159.

[13] Q.Y. Zhang, L.T. Wang, and X.H. Wang, Influence of casting speed variation during unsteady continuous casting on non-metallic inclusions in if steel slabs, *ISIJ Int*., 46(2006), No. 10, p. 1421.

[14] Y.R. Liu, D. Ye, Q.L. Yong, J. Su, K.Y. Zhao, and W. Jiang, Effect of heat treatment on microstructure and property of Cr13 super martensitic stainless steel, *J. Iron Steel Res. Int*., 18(2011), No. 11, p. 60.

[15] Z.L. Song, X.D. Du, Y.Q. Chen, J.Q. Wang, C. Ye, and L.Y. Li, Microstructure and impact toughness of 7Cr17Mo martensitic stainless steel, *Trans. Mater. Heat Treat*., 32(2011), No. 5, p. 95.

[16] J.Y. Li, P. Zhao, J. Yanagimoto, S. Sugiyama, and Y.L. Chen, Effects of heat treatment on the microstructures and mechanical properties of a new type of nitrogen-containing die steel, *Int. J. Miner. Metall. Mater.*, 19(2012), No. 6, p. 511.

[17] L.D. Barlow and M.Du. Toit, Effect of austenitizing heat treatment on the microstructure and hardness of martensitic stainless steel AISI 420, *J. Mater. Eng. Perform*., 21(2012), No. 7, p. 1327.